Influence of operating speed on the thermo-mechanical behaviour of cylindrical roller bearing

Themba Mashiyane[a]*, Dawood Desai[a], Lagouge Tartibu[b]

[a] *Department of Mechanical and Mechatronics Engineering, Tshwane University of Technology, Pretoria, South Africa*
[b] *Department of Mechanical and Industrial Engineering Technology, University of Johannesburg, South Africa*
Corresponding author*: tmashiyane12@gmail.com

Abstract

The high load-bearing ability of cylindrical roller bearing made its usage in rotating machinery popular. However, the performance of this bearing is impeded by the contact stress, stiffness and the temperature rise experienced operation. In this study, the thermo-mechanical behaviour of martensitic stainless steel (X20) fabricated roller bearing with polyamide pin-type cage subjected to different rotating/operating speeds was simulated using finite element analysis software, Abaqus. The outcome of the analyses shows that the temperature, heat flux, contact or Hertzian stress and frictional energy developed in the bearing during operation increases with a corresponding increase in speed. It was further observed that a slight increase in the operating speed of the bearing leads to a significant rise in the temperature and frictional energy developed in the bearing. Also, the maximum Hertzian/contact stress was observed to developed on the outer ring of the roller bearing assembly (at the point of contact between the outer ring and the balls) in all the operational speeds considered. Thus, making this outer ring more susceptible to failure during operation as compared to the other components of the bearing.

Keywords: Abaqus, contact, friction, Hertzian stress, heat flux, polyamide

1.   Introduction

Ball and roller bearing, also known as rolling bearing are engineering components that are frequently used in rotating machinery where they function primarily as a support system (Sharma et al., 2018, Sharma et al.). Rolling components are designed to pose high carrying capacity, high strength and low-frictional properties which enable them to serve different engineering purposes (Sharma et al.). Thus, they are utilized in applications that require rotational motion or a component revolving around a shaft in a simple industrial or machinery device. An example of a simple industrial and commercial application of bearing includes electric motors, bicycles, wheels, and roller skates (Ricci, 2010). Similarly, they are utilized in complex engineering machinery applications such as gyroscopes, aircraft/power generation gas turbines, dental drills, power transmission and rolling drills (Ricci, 2010). Due to the conditions of application of roller bearings (exposure to cyclic loading), they often experience engineering failure as a result of different thermo-mechanical reasons. Among these are inherent materials defects developed during fabrication, working conditions, heat generation, high contact/Hertzian stress development and vibration (Ricci, 2010). More often, engineering failure due to bearing collapse mostly lead to breakdown and sometimes catastrophic failure of the equipment. Several bearings are available in the market, and radial bearings are considered one of the most important components in industrial applications because they are suitable and easily adaptable in various machinery (Shao et al.). Other types of bearing used in machinery include thrust bearings, spherical bearings, cylindrical roller bearings and tapered roller bearings (Upadhyay et al., 2013). Of all these bearings, a cylindrical roller bearing of the same size as the other bearings has a higher load-bearing capacity, as such, it is frequently used in moderate speed and heavy-duty applications (Sehgal et al., 2000, Upadhyay et al., 2013).

In addition, cylindrical roller bearings come in different sizes and types, thus, they are versatile in their applications (Sehgal et al., 2000). They are designed such that the rollers are guided by the side of one of the rings, and are easily removable due to the presence of ring collar and cage. This type of design usually eases the mounting and dismounting of bearings, especially in applications that require tight-fitting of both rings because of the loading conditions. The importance of bearings cannot be overemphasized because they are designed to poses high strength properties, withstand high complex loadings and function in high-cost machinery (Sehgal et al., 2000). Thus, they have received remarkable attention that encourages the manufacturing of durable and long-life span bearings.

Based on the understanding that bearings are critical components of high-speed precision ball–screw systems, the smooth operations of machinery depends on them. There exist several connections that support the roller bearings during operations, most notable are the interfaces between the connecting shaft and bearing and bearing cage support (Deng et al., 2014). Contact friction at the connection point or joints is developed between two surfaces in contact regardless of the amount of pressure exacted between them. Consequently, the activities of friction generate heat, which results in a rise in temperature, an event that is detrimental to the structural and material properties of the bearing. The increase in temperature experienced during operation often lead to overheating of the coolant, and the occurrence of mechanical micro-deformations (Reddy, 2015). Hence, the development of high temperature during

the operation of a roller bearing leads to overheating, a process that significantly influences the thermal behaviour of the bearing system (Reddy, 2015).

To comprehend and hereafter explain the thermo-mechanical behaviour of roller bearing due to operating conditions, numerous studies and approaches have been implemented theoretically and experimentally (Reddy, 2015). Nevertheless, experimental methods are quite expensive and are often hindered by various unpredictable factors (Shao et al.). Hence, different researchers have conducted several theoretical analyses in order to establish the dynamic behaviour of bearing systems, and considerations were given to operating conditions and inherent defects in the materials (Shao et al.).

Therefore, this study attempted to investigate the influence of operating speeds on the thermo-mechanical behaviour of a defect-free cylindrical roller bearing using finite element analysis software, Abaqus.

2. Dynamic loading and heat generation in bearings

When a bearing is subjected to dynamic loading during operation, heat is often generated due to the friction between two or more components of the bearing (Petrov and Lavrentyev, 2019). The dynamic loading and heat generated in the different components of a roller bearing are presented in subsequent subsections.

2.1 Loading of bearings

In the event where the size of bearings used in a component is been determined with other factors rather than load, the loading of such bearing is done based on its size and load-carrying capacity. If very light loads are applied on a bearing, failure due to fatigue becomes less prevalent, while raceways skidding or smearing and cage damage appear to be the dominant failure mechanisms. Therefore, a minimum load must always be applied on a roller bearing if a satisfactory operating condition must be attained. For a bearing with spherical balls, the minimum loads it must be subjected to is given as: $P_m = 0.01C$ while for bearings with cylindrical balls, the minimum load is given as: $P_m = 0.02C$.

where P_m is the minimum load a bearing must be subjected to (kN), C represents the basic static load rating (kN).

2.2 Lifespan of bearing

The appropriate estimation of the useful life of bearing under specified service operation is paramount as it allows for the timely replacement of failing components. To accurately estimate the hours or number of cycles a bearing would survive before failure, resulting from fatigue, the equivalent dynamic radial loading of such bearing must be known as the value account for both the axial and radial stresses. For a loaded bearing acted upon simultaneously by an axial load (F_a) and a radial load (F_r) that has a fixed magnitude and direction, the equivalent dynamic load P can be estimated as follow:

$$P = XF_r + YF_a \tag{1}$$

where P represents the bearing's equivalent dynamic load (kN), Fr represents the axial load (kN), F_a represents the radial load in (KN), and the radial and axial loading factors are represented by X and Y respectively.

For bearings like needle roller thrust bearing, thrust ball bearings, cylindrical bearings etc, allow only axial loads. Thus, a simplified dynamic load is obtained provided that the load acts centrically, and the equivalent dynamic load is given as:

$$P = F_a \tag{2}$$

2.3 Analysis of bearing motion

If a spherical bearing is loaded radially, and the inner ring rotates at an angular velocity ω_i, causing the cage and cylindrical balls to rotate at an angular velocity ω_c about the axis of rotation, and the cylindrical balls revolving along their axis at an angular velocity ω_r.

Since roller bearings are frequently used in heavy load and low-speed applications, the skid between the raceways and rollers are often negligible, and the roller-raceway relationship is assumed to be pure rolling (Deng et al., 2014, Ma et al., 2016). Therefore, the roller-inner raceway and roller-outer raceway average linear velocity can be expressed as follows (Ma et al., 2016):

$$U_i = 0.5d_m \left[(1 - \gamma)(\omega_i - \omega_c) + \left({}^D/_{d_m} \right) \omega_r \right] \tag{3}$$

$$U_o = 0.5d_m \left[(1 + \gamma)\omega_c + \left({}^D/_{d_m} \right) \omega_r \right] \tag{4}$$

where d_m represents the pitch diameter of roller or ball, D represents the roller diameter, $\gamma = \frac{D}{d_m} \cos \alpha$, α is normal contact angle, ω_i represents the inner ring angular velocity (rad/s), ω_c represents the cage's angular velocity (rad/s), ω_r represents the roller's angular velocity about its axis (rad/s) and the average linear velocity of the inner and outer roller-runway is represented by U_i and U_o, respectively.

2.4 Heat generation in roller bearing

Since the cage of a roller bearing rides on the surface of the inner ring, a force, F_{CS} is formed between the two surfaces (inner ring surface and the cage). This force can be computed using Petroff's law (Harris and Kotzalas, 2006) as follow,

$$F_{CS} = \frac{2\pi \varphi b_c r_c^2 (\omega_i - \omega_c)}{\delta_c} \tag{5}$$

and the heat generated, H_{CS} due to the frictional effect between the two surfaces can be calculated as,

$$H_{CS} = 0.5d_m F_{CS}(\omega_i - \omega_c) \tag{6}$$

2.5 Heat generation due to roller-cage pocket contact

The frictional force, F_P developed due to roller-cage pocket contact is given as (Pouly et al., 2010)

$$F_P = \frac{2\pi \varphi l_P b_P^2 \omega_r}{\delta_P} \tag{7}$$

Table 1: Dimensions of components of the cylindrical roller bearing (Mashiyane et al., 2021, Mashiyane et al., 2022)

Outer ring (mm)			Inner ring (mm)			Cage (mm)			Cylindrical ball (mm)	
Diameter		Height	Diameter		Height	Diameter		Height	Diameter	Height
Internal	External		Internal	External		Internal	External			
91.4	110.0	27.0	50.0	65.0	24.0	71.5	87.5	24.0	14.5	16.0

For Z roller-cage pocket contacts, the total heat generation rate is given as

$$H_P = ZDF_P\omega_r \qquad (8)$$

where Z represents the number of rollers, I_P represents the axial length of the cage pocket and φ represents the dynamic viscosity of the lubricant oil, b_P represents the width of elliptic point contact and the roller and cage clearance is represented with δ_P.

2.6 Heat generated by roller churning

In the presence of air and lubricant, the drag force exerted on a roller rotating around a shaft that results in heat generation can be expressed as follow (Deng et al., 2014):

$$F_d = \frac{1}{8}C_d\rho Dl_e(d_m\omega_c)^2 \qquad (9)$$

where C_d represents the coefficient of the roller drag force, d_m represents the mass density of the air mixture and lubricant in the housing, F_d represents the drag force (N) and the roller's effective length is represented by I_e .

Thus, the expression for the total heat H_d, generated in Z roller churning is given as:

$$H_d = 0.5ZF_d d_m\omega_c \qquad (10)$$

2.7 Heat generation due to roller-raceway contact

By integrating the product of the slicing linear velocity of the roller and the lubricating shear velocity of the roller-raceway, the total heat generated H_{RR} due to the roller-raceway contact can be obtained (Wang, 2013, Ma et al., 2016).

2.8 Total heat generated in spherical roller bearing

Since a spherical roller bearing consists of a cage, rollers/cylindrical balls, inner and outer ring, the total heat generated H_{Tot} in the bearing can be obtained as follow:

$$H_{Tot} = H_d + H_{CS} + H_P + H_{RR} \qquad (11)$$

3. FE model and analysis

Finite element (FE) analysis software, Abaqus was used in this study to develop the model, and also determine the effect of operational/rotational speed of the thermo-mechanical behaviour of the cylindrical roller bearing.
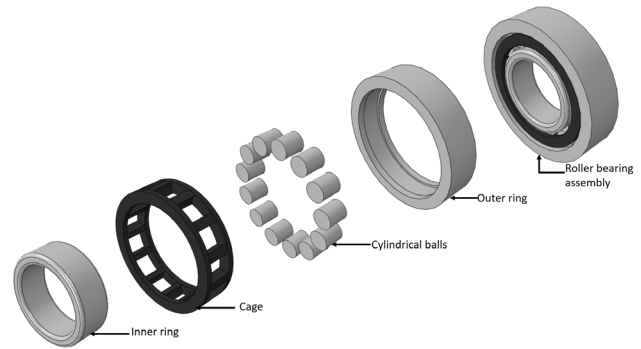
Figure 1: Parts and assembly model of roller bearing

3.1 Model development

A cylindrical roller bearing with 13 cylindrical balls, inner ring, outer ring and the pin-type cage was developed using finite element analysis software, Abaqus (Systemes, 2013, Ogunbiyi et al.). The inner, outer ring and cylindrical balls are made of martensitic stainless steel such as X20 (Noury and Eriksson, 2017) because of their high strength and excellent creep resistance at high temperature, while the pin-typed cage is made of a lightweight material, polyamide 66 also known as Nylon (SKF-Group, 2019), since the primary function of the cage is to prevent the balls from having direct contact with one another during operation. **Figure 1** illustrates the parts and assembly model of the roller bearing while **Table 1** shows the dimensions of the inner, outer ring, cage and cylindrical balls.

X20 martensitic stainless steel material properties used for the fabrication of the inner, outer ring, cylindrical bearing, and the polyamide 66 used for the cage is depicted in **Table 2**.

Table 2: Material properties for components of the cylindrical roller ball bearing (Salifu et al., 2020f, Salifu et al., 2020e, Salifu et al., 2020a, Hlebanja et al.).

Material properties	Polyamide (Cage)	X20 steel
Density (kg/m³)	1 310	7 800
Elasticity (GPa)	2.95	200
Poisson's ratio	0.41	0.28
Specific heat capacity (J/kgK)	1 680	46
Thermal expansion	6.60	1.00
Thermal conductivity (W/m²)	0.25	28.00

In order to keep the balls, cage, inner and outer ring in contact, appropriate coupling interaction with a general coefficient of friction of 0.02 was applied on the assembly. Furthermore, dynamic explicit step was applied in the analysis and mechanical boundary conditions were applied to the assembly such that it can undergo displacement and rotation as depicted in **Figure 2**. In the applied
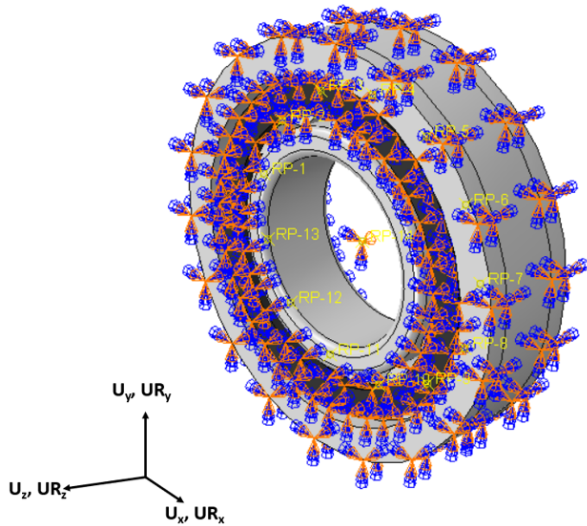
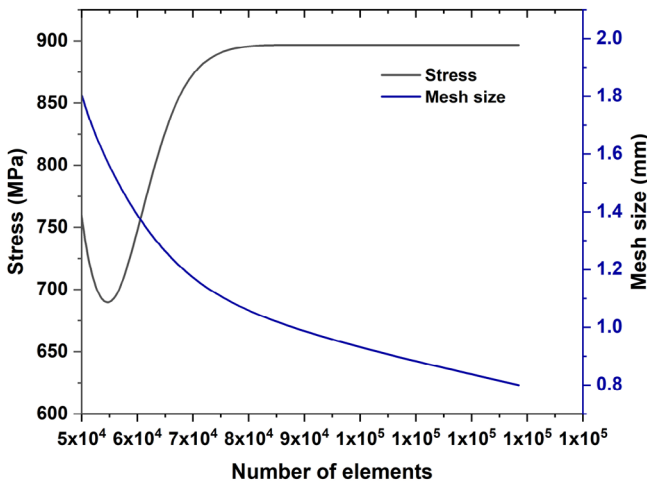**Figure 2:** Mechanical boundary conditions applied

Figure 3: Mesh convergency study graph

mechanical boundary conditions, the outer ring is fixed while the inner ring, balls and cage are allowed to undergo displacement in U_x, U_y and U_z direction, and rotation in the UR_x, UR_y and UR_z direction. The inner ring is subjected a fixed body load of 160 kN while the cylindrical balls and inner ring are subjected to three different angular velocities, (157, 300 and 503 rad/s).
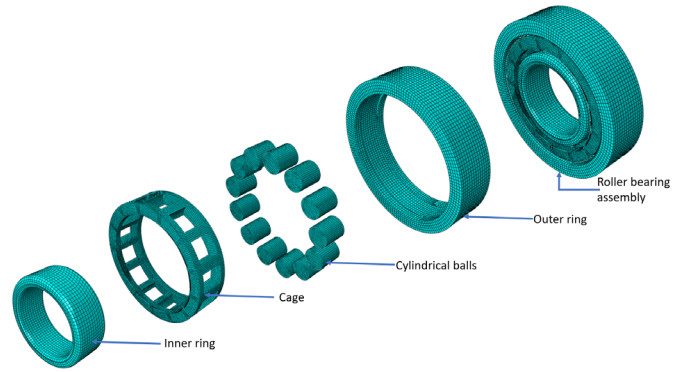

Figure 4: Part and assembly mesh of cylindrical roller bearing

The bearing assembly has a total of 83 230 linear hexagonal elements of type C3D8T consisting of 105 285 nodes. 5 2508 of the total elements is from the inner ring, 26 688 is from the cage, 9 734 is from the outer ring while the 13 cylindrical balls have a total of 41 600 elements. After conducting mesh convergence studies (Salifu et al., 2019, Salifu et al., 2020b, Salifu et al., 2020f, Salifu et al., 2020d, Salifu et al., 2020c, Salifu et al., 2021, Babalola et al., 2020) as depicted in **Figure 3**, the cylindrical balls and the cage were meshed with 1 mm mesh size while the outer and inner ring were meshed with 2 mm mesh size. The use of 1 mm mesh size for the entire component of the bearing would produce a similar result but at a prolonged computational time. Thus, the use of 2 mm mesh size for the bigger components (inner and outer ring). The parts and assembly mesh of the roller bearing after applying the above mesh sizes is shown in **Figure 4**.

4. Results and discussions

Due to friction between the surfaces in contact in the cylindrical roller bearing, the temperature developed in the bearing was observed to increase with an increase in operational speed. Depicted in **Figure 5** is the contour plot of the temperature distribution profile obtained when the roller bearing is subjected to an operational speed of 157, 300 and 503 rad/s, respectively while the plot of their corresponding heat flux is shown in **Figure 6**.

The temperature distribution profile of the three operational speeds considered shows that the maximum temperature is developed
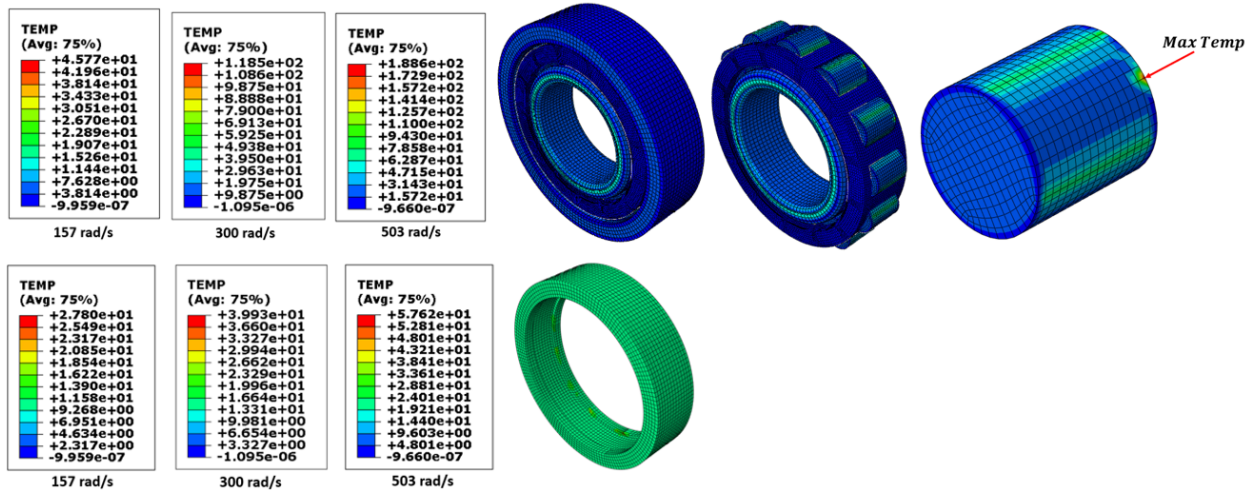

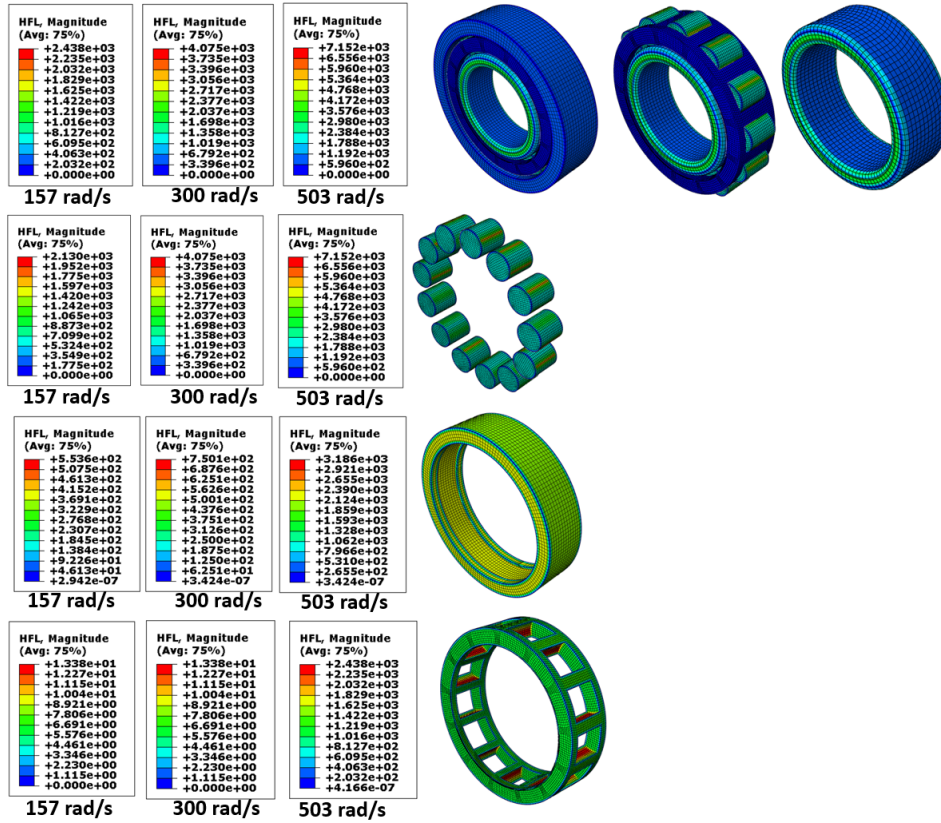**Figure 5:** Temperature distribution profile of the different operating speeds

Figure 6: Contour plot of the heat flux developed for the different operating speeds
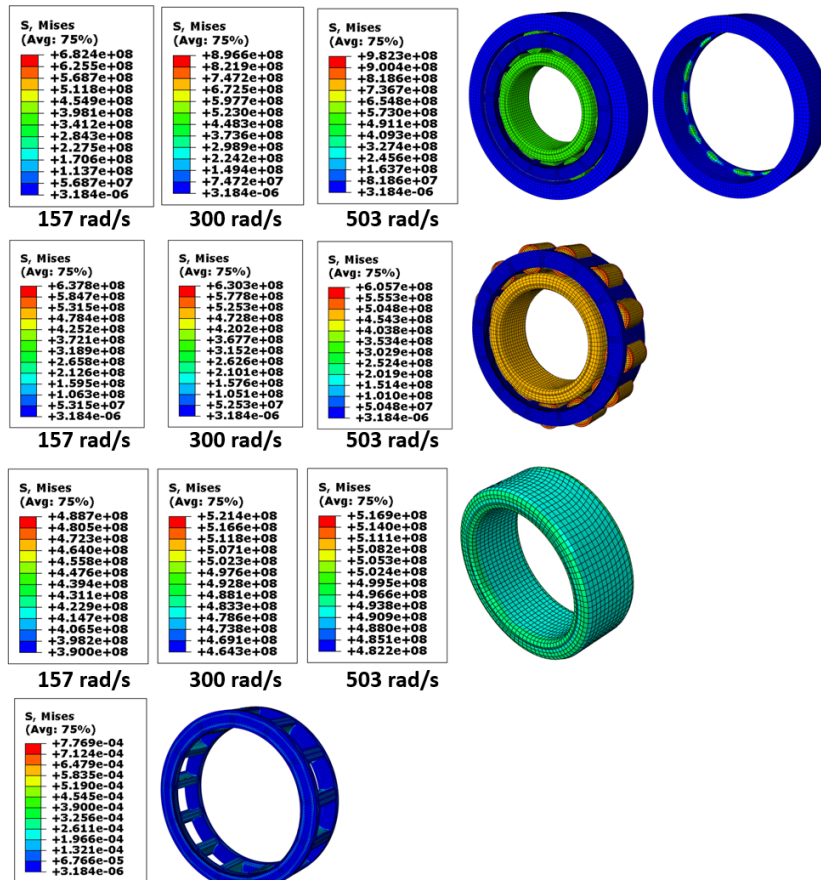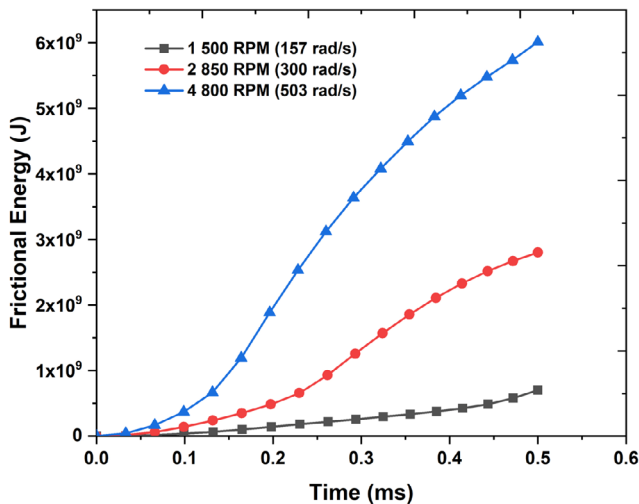

Figure 7: Stress distribution profile contour plot for the different operating speeds

Figure 8: Frictional energy of the roller bearing under the different speeds

on the tip of the cylindrical bearing, where there is possible contact between the balls and the inner ring. Furthermore, the developed temperature was observed to increase with an increase in operational/rotational speed such that the analysis with an operational speed of 157 rad/s developed the least temperature (45.77 ℃), while the analysis with an operational speed of 503 rad/s developed the highest temperature (188.6 ℃) under the same operating time. Hence, it is worth noting that a slight increase in the operating/rotational speed has a significant effect on the value of temperature developed in the assembly, since the contact between the rotating components of the assembly, due to friction leads to a rise in temperature, thermal expansion and possible stiffness of the bearing during operation (Venkatesh and Prasad, 2017).

Similarly, the heat flux developed across the different components the roller bearing is made of was observed to increase with an increase in the operating speed. As expected, the least heat flux was developed on the cage, since it is the only non-metallic component in the assembly with the least interaction during operation in the entire assembly.

Just like the temperature and heat flux distribution profile, the contact stress, also known as Hertzian stress developed in the roller bearing assembly increases with an increase in operating/rotating as depicted in Figure 7. From the figure, the maximum Hertzian stress in the three operating speeds considered was developed on the outer ring, at the points of contact between the cylindrical balls and the outer ring. The maximum contact or Hertzian stress developed for analysis with 157, 300 and 503 rad/s are 682.4, 896.6 and 982.3 MPa, respectively. Furthermore, the least stress was developed on the cage due to its minimal interference in the whole process as compared to the other components. A similar result was reported by Pușcașu et al. (2017), where the maximum Hertzian stress in the bearing assembly was developed on the outer ring.

The value of the Hertzian or contact stress developed in the roller bearing when subjected to the different operating speed/rotation shows that the analysis with the highest operating speed (503 rad/s) developed tend to fail quicker than the ones with lesser operating/

rotating speed, and the failure would emanate from the outer ring (point of contact between the outer ring and the cylindrical balls).

Due to the contact between the parts that make up the roller bearing assembly, frictional energy is developed during operation. Depicted in **Figure 8** is a plot of the frictional energy developed in the roller bearings under the different operating/rotating speeds. Just like the results obtained from the other analysis, the frictional energy increases with an increase in the operating/rotational speed. The increasing values of the frictional energy with operating/rotating speed and time is a direct result of the thermal expansion of the components that makes up the bearing during operation, and this in return leads to stiffness (Venkatesh and Prasad, 2017).

Conclusion

The FE analysis results obtained in this study when the roller bearing was subjected to different operating speeds show that the temperature, heat flux, Hertzian stress and frictional energy increases with an increase in operating/ rotating speed, such that the maximum temperature was developed at the tip of the cylindrical bearings (at the point of contact between the balls and the inner ring), while the maximum Hertzian stress was developed on the point of contact between the balls and the outer ring. Hence, the outer ring is most more prone to failure in the entire bearing assembly since the highest Hertzian stress was developed on this component during operation.

Also, the study shows that the operational/rotating speed of a roller bearing during service plays a greater role in the temperature, heat flux, Hertzian stress and frictional energy developed in components because the higher the operational/rotational speed, the higher the value of the Hertzian stress developed, and the faster the likelihood of failure of the components of the bearing.

Finally, the use of this FE technique allows for the early identification of the components of the bearing that is most prone to failure when subjected to different operating speeds.

Acknowledgements

References

1. BABALOLA, B. J., SALIFU, S. & OLUBAMBI, P. A. 2020. Effect of Mechanical Milling on the Mechanical, Dry Sliding Wear, and Impact Response of Sintered Nickel Based Superalloy. *Journal of Materials Engineering and Performance,* 29**,** 8348-8358.
2. DENG, S. E., JIA, Q. Y. & XUE, J. X. 2014. Design principles of rolling bearings. *Standards Press of China, Beijing.*
3. HARRIS, T. A. & KOTZALAS, M. N. 2006. *Advanced concepts of bearing technology: rolling bearing analysis*, CRC press.
4. HLEBANJA, G., HRIBERŠEK, M., ERJAVEC, M. & KULOVEC, S. Durability Investigation of plastic gears. 2019. EDP Sciences, 02003.
5. MA, F., LI, Z., QIU, S., WU, B. & AN, Q. 2016. Transient thermal analysis of grease-lubricated spherical roller bearings. *Tribology International,* 93**,** 115-123.
6. MASHIYANE, T., DESAI, D. & TARTIBU, L. 2021. Finite Element Analysis of the Thermo-mechanical Behaviour of Defect-Free Cylindrical Roller Bearing in Operation. *Arabian Journal for Science and Engineering,* 1-11.

7. MASHIYANE, T., DESAI, D. & TARTIBU, L. 2022. Dynamic analysis and frequency response of cylindrical roller bearing of an airflow root blower. *Cogent Engineering,* 9**,** 2021837.

8. NOURY, P. & ERIKSSON, K. 2017. Failures of high strength stainless steel bridge roller bearings: A review. *Engineering Fracture Mechanics,* 180**,** 315-329.

9. OGUNBIYI, O. F., SALIFU, S. A., JAMIRU, T., SADIKU, E. R. & ADESINA, O. T. Thermo-mechanical simulation of steam turbine blade with spark plasma sintering fabricated Inconel 738LC superalloy properties. 2019. IOP Publishing, 012046.

10. PETROV, N. I. & LAVRENTYEV, Y. L. 2019. Empirical correlation of heat generation in ball bearings depending on the operational conditions in the supports of aero-engine rotor. *IOP Conference Series: Materials Science and Engineering,* 489**,** 012029.

11. POULY, F., CHANGENET, C., VILLE, F., VELEX, P. & DAMIENS, B. 2010. Power Loss Predictions in High-Speed Rolling Element Bearings Using Thermal Networks. *Tribology Transactions,* 53**,** 957-967.

12. PUȘCAȘU, A. M., LUPESCU, O. & BĂDĂNAC, A. Analysis of cylindrical roller bearings design in order to optimize the classical process using FEM. 2017 2017. EDP Sciences, 06017.

13. REDDY, M. C. S. 2015. Thermal Stress Analysis of a Ball Bearing by Finite Element Method. *International Journal of Advanced Research in Engineering and Technology,* 6.

14. RICCI, M. 2010. Static load distribution in ball bearings including the effects of temperature and fit. *WIT Transactions on Engineering Sciences,* 66**,** 223-234.

15. SALIFU, S., DESAI, D., FAMESO, F., OGUNBIYI, O., JEJE, S. & ROMINIYI, A. 2020a. Thermo-mechanical analysis of bolted X20 steam pipe-flange assembly. *Materials Today: Proceedings.*

16. SALIFU, S., DESAI, D. & KOK, S. 2020b. Comparative evaluation of creep response of X20 and P91 steam piping networks in operation. *The International Journal of Advanced Manufacturing Technology,* 109**,** 1987-1996.

17. SALIFU, S., DESAI, D. & KOK, S. 2020c. Creep–fatigue interaction of P91 steam piping subjected to typical start-up and shutdown cycles. *Journal of Failure Analysis and Prevention.*

18. SALIFU, S., DESAI, D. & KOK, S. 2020d. Numerical investigation of creep-fatigue interaction of straight P91 steam pipe subjected to start-up and shutdown cycles. *Materials Today: Proceedings.*

19. SALIFU, S., DESAI, D. & KOK, S. 2020e. Numerical simulation and creep-life prediction of X20 steam piping. *Materials Today: Proceedings.*

20. SALIFU, S., DESAI, D. & KOK, S. 2020f. Prediction and comparison of creep behavior of X20 steam plant piping network with different phenomenological creep models. *Journal of Materials Engineering and Performance***,** 1-14.

21. SALIFU, S., DESAI, D. & KOK, S. 2021. Determination of the dominant failure mechanism of P92 steam piping subjected to daily operational cycle using finite element (FE) technique. *Suid-Afrikaans Tydskrif vir Natuurwetenskap en Tegnologie/South African Journal of Science and Technology,* 40**,** 37-43.

22. SALIFU, S., DESAI, D., KOK, S. & OGUNBIYI, O. 2019. Thermo-mechanical stress simulation of unconstrained region of straight X20 steam pipe. *Procedia Manufacturing,* 35**,** 1330-1336.

23. SEHGAL, R., GANDHI, O. P. & ANGRA, S. 2000. Reliability evaluation and selection of rolling element bearings. *Reliability Engineering & System Safety,* 68**,** 39-52.

24. SHAO, Y., TU, W. & GU, F. A simulation study of defects in a rolling element bearing using FEA. 2010. IEEE, 596-599.

25. SHARMA, A., AMARNATH, M. & KANKAR, P. K. Effect of unbalanced rotor on the dynamics of cylindrical roller bearings. 2015. Springer, 1653-1663.

26. SHARMA, A., AMARNATH, M. & KANKAR, P. K. Effect of varying the number of rollers on dynamics of a cylindrical roller bearing. 2014. American Society of Mechanical Engineers, V008T11A067.

27. SHARMA, A., UPADHYAY, N., KANKAR, P. K. & AMARNATH, M. 2018. Nonlinear dynamic investigations on rolling element bearings: A review. *Advances in Mechanical Engineering,* 10**,** 1687814018764148.

28. SKF-GROUP. 2019. *Components and materials* [Online]. Sweden: SKF Group. Available: https://www.skf.com/africa/en/products/rolling-bearings/principles-of-rolling-bearing-selection/general-bearing-knowledge/bearing-basics/components-and-materials [Accessed 11/05/2021 2021].

29. SYSTEMES, S. D. 2013. ABAQUS 6.13 User's manual. *Dassault Systems, Providence, RI.*

30. UPADHYAY, R. K., KUMARASWAMIDHAS, L. A. & AZAM, M. S. 2013. Rolling element bearing failure analysis: A case study. *Case studies in engineering failure analysis,* 1**,** 15-17.

31. VENKATESH, K. & PRASAD, K. R. 2017. Finite Element Solution for Thermal Analysis of NiTiNOL-60 Ball Bearing.

32. WANG, L. Q. 2013. Design and numerical analysis of rolling element bearing for extreme applications. Harbin: Harbin Institute of Technology Press.